

# Composite states of wetting

Joël De Coninck<sup>(1)</sup>, François Dunlop<sup>(2)</sup> and Thierry Huillet<sup>(2)</sup>

<sup>(1)</sup>Laboratoire de Physique des Surfaces et Interfaces  
Université de Mons, 20 Place du Parc, 7000 Mons, Belgium

<sup>(2)</sup>Laboratoire de Physique Théorique et Modélisation  
CY Cergy Paris Université, CNRS UMR 8089,  
95302 Cergy-Pontoise, France

October 22, 2020

## Abstract

The analytical expressions of liquid-vapor macroscopic contact angles are analyzed for various simple geometries and arrangements of the substrate, in particular when the latter exhibits two or more scales. It concerns the Wenzel state of wetting when the substrate is completely wet, the Cassie-Baxter state when the liquid hangs over the substrate, but also intermediate states of wetting which are shown to be relevant and in competition with the two other ones. Under a separation of scales hypothesis, a composition rule of contact angles is developed whose interest is illustrated in a close packing setup of raspberry-like particles.

## 1 Introduction and outline of the results

Superhydrophobicity refers usually to a surface which is sufficiently rough to have a water droplet suspended on top of the roughness features, with air trapped underneath corresponding thus to a water-air interface. Several approaches have been proposed to design such surfaces by creating micro/nanostructures on hydrophobic surfaces. About the corresponding techniques let us mention crystallization control [1], phase separation [2], template synthesis [3, 4], electrochemical deposition [5], and chemical vapor deposition [6]. Another way to proceed is to coat or graft micro/nanostructured hydrophilic surfaces with hydrophobic molecules [7, 8, 9]. Such materials include fluoroalkylsilanes [10], fluoropolymers [11], other organic polymers [12], and alkylketene dimers [13]. To date, various initially hydrophilic substrates such as metal, glass, silicon wafer, and fabric have been used to prepare superhydrophobic surfaces in this way.

Among these techniques, one of the most popular method is to deposit one or two layers of nanoparticles on top of the base surface and to fix them by one way

or another (sol-gel, annealing, grafting, ...). The advantage of this last technique is that it is cheap and simple to process. Many examples can be found in the literature [14, 15]. However what is not clear is what kind of nanoparticles should be used to enhance the superhydrophobic effect? This question has been addressed by many experimentalists where authors have considered several aspect ratios for one or two layers of nanoparticles [16]. The purpose of the present work is to provide a thorough modelling of such complex wetting states.

Wetting issues have been addressed in a simplistic two-scale roughness model in 1+1 dimensions [17]. Composite states of wetting are already meaningful in this setup, together with the separation of scales idea; see also [18] for a randomized setup and the robustness problem of superhydrophobicity with respect to disorder.

In Section 2, we discuss the problem of computing the Wenzel roughness  $r$  for a 2-scale substrate, as a function of the roughnesses  $r_1, r_2$  of both scales separately. We find general conditions for  $r = r_1 r_2$  or for  $r = r_1 + r_2 - 1$ . Then

$$\cos \theta^W = r \cos \theta_0,$$

where  $\theta^W$  is the Young angle of a drop in the Wenzel (completely wet) state and  $\theta_0$  the Young angle for a flat surface of the same material.

In Section 3, we discuss the Cassie-Baxter covered fraction  $\phi$  with the liquid-vapor interface lying in a unique horizontal plane. With  $r^{wet}$  the roughness of the wetted part of the substrate, we extend the validity of the corresponding Young equation for the Cassie-Baxter contact angle:

$$\cos \theta^{CB} = -1 + \phi (1 + r^{wet} \cos \theta_0).$$

In Section 3.1, we ask whether the liquid-vapour interface is stable, metastable or unstable, following questions raised by Marmur [19] who showed stability for convex solids. His stability conclusions are extended to include more general shapes that we call ‘vertically convex’.

In Section 3.2, we investigate whether  $\phi = \phi_1 \phi_2$  for the Cassie-Baxter wetting of 2-scale substrates for which  $r = r_1 + r_2 - 1$  and with a roof-top structure at small scale on top of the one at the larger scale. In this setup, under some restrictive hypothesis, composite states of wetting can be defined in a natural way, together with their contact angles.

In Section 4, the separation of scales hypothesis is introduced, allowing to define a composition rule of contact angles. Subsection 4.1 deals with the case of a 2-scale affine roughness situation, while Subsection 4.2 focuses on the 3-scale case. In Subsection 4.3 a situation with isotropic roughness is considered, still under the separation of scales hypothesis. For some particular geometries, the expression of the composition rule for contact angles is developed. This includes the case of a close packing of raspberry-like particles.

As an input to the previous 2-scale models, Section 5 is devoted to 1-scale models, with patterns obeying cylindrical symmetry. Subsection 5.1 concerns monodisperse spherical particles. Under such hypothesis, the contact angle  $\theta^{CB}$  of the Cassie-Baxter state is computed, together with the contact angle  $\theta^W$  of

the quasi-Wenzel state, which has some air trapped at the basis of the spheres (small region bounded by a catenoid). Subsection 5.2 deals with monodisperse cylindrical pillars, also possibly with air trapped below catenoids.

## 2 Wenzel roughness

The Wenzel roughness or specific surface area  $r$  is defined as the true substrate area divided by the projected area. The definition applies to a surface or piece of a surface which is plane at the macroscopic scale. The projection is onto the corresponding plane, so that the projected area is also simply the area on the macroscopic scale. The definition can be applied to any surface whose boundary is a plane curve. The macroscopic surface is a plane domain  $\Omega \subset \mathbb{R}^2$ , of area  $|\Omega|$  and piecewise smooth boundary  $\partial\Omega$ . The real substrate is a surface  $S$  embedded in  $\mathbb{R}^3$  with the same boundary  $\partial\Omega$  as the macroscopic domain. The surface  $S$  should be self-avoiding. We assume  $S$  to be piecewise smooth. Experimentally, there is a scale length below which  $S$  is considered smooth. This scale is part of the definition of the Wenzel roughness. We then define the Wenzel roughness as  $r = \lim_{\Omega \nearrow \mathbb{R}^2} \int_S dS / |\Omega|$ . Note that  $|\Omega|$  may be slightly different from the projected area of  $S$ , due to overhangs at the boundary, which should be negligible in the thermodynamic limit or may be absent altogether. For  $r$  to be uniquely defined, the sample should be large on a microscopic scale. In a microscopic model, one should take the limit as the area tends to infinity, unless the real surface is periodic so that one cell is enough to compute. If the roughness is random, the existence of the limit requires a law of large numbers, which essentially requires independence between distant points on the substrate.

As an example, partition the plane into squares of side  $a$ . In the center of each square grow a pillar of square section of fixed side  $a_1 < a$  and random height  $b_{1,i}$ , where  $i$  labels the pillar or the corresponding square. The area is

$$S = \sum_i (a^2 + 4a_1 b_{1,i}) \quad (1) \quad \boxed{\text{S1}}$$

Assume the  $b_{1,i}$  identically distributed, with mean  $\bar{b}_1$ . The Wenzel roughness is

$$r_1 = \lim_{\Omega \nearrow \mathbb{R}^2} \frac{S}{|\Omega|} = \lim_{\Omega \nearrow \mathbb{R}^2} \frac{\sum_i (a^2 + 4a_1 b_{1,i})}{\sum_i a^2} = 1 + 4 \frac{a_1 \bar{b}_1}{a^2} \quad (2) \quad \boxed{\text{r1}}$$

where the last step is the law of large numbers, easily satisfied if the  $b_{1,i}$  are asymptotically independent at large distances. A special case is  $b_{1,i}$  taking some fixed value  $b_1$  with probability  $p$  and value 0 (no pillar) with probability  $1 - p$ , so that  $\bar{b}_1 = pb_1$ .

If the real surface has (Hausdorff) dimension 2, not a fractal, then the Wenzel roughness is scale invariant, as in (2). If the surface is defined by a single length, then the Wenzel roughness is independent of this length. For example a surface made by a compact arrangement of monodisperse spheres upon a plane has a roughness independent of the sphere radius.

In the completely Wenzel state the substrate is completely wet, with no air trapped at all. The corresponding contact angle  $\theta^W$  is easily shown to obey

$$\cos \theta^W = \lim_{\Omega \nearrow \mathbb{R}^2} \frac{S(\gamma_{SV} - \gamma_{SL})}{|\Omega| \gamma_{LV}} = r \cos \theta_0, \quad \text{if } r \leq 1/|\cos \theta_0|, \quad (3) \quad \boxed{\text{wenzel}}$$

whatever the geometry [28]. The angle  $\theta_0$  is the Young angle for a flat surface of the same material. If  $r \cos \theta_0 \geq 1$ , complete wetting occurs. If  $r \cos \theta_0 \leq -1$  then the completely Wenzel state is not the minimizer of free energy. Indeed minimizing free energy is equivalent to maximizing the cosine of the apparent contact angle, and Cassie-Baxter configurations will have  $\cos \theta^{CB} > -1$ .

Measuring  $r$  may be difficult. Parts of the real surface may be hidden by overhangs. The Wenzel roughness of superhydrophobic films built from raspberry-like particles [20] is under-estimated by optical apparatus.

In section 5.1 we shall see almost Wenzel states, with a little air trapped below spherical particles, implying a deviation from Wenzel's law (3).

## 2.1 Two scales of roughness, $r = r_1 r_2$ ?

$\boxed{\text{rr1r2}}$

There may be two or more mesoscopic scales of roughness, separated say by an order of magnitude. Here we examine the possibility that  $r = r_1 r_2$ . At the first, larger, scale of roughness, one has a surface  $S_1$  embedded in  $\mathbb{R}^3$  with the same boundary  $\partial\Omega$  as the macroscopic domain. The second, smaller, scale of roughness is not visible, so that  $S_1$  is piecewise smooth and  $\int_{S_1} dS_1 = r_1 |\Omega|$ . Now each  $dS_1$  may be enlarged so that the second scale becomes visible, and the true surface with the same boundary as  $dS_1$  has an area  $r_2 dS_1$ . The true total area is  $\int_{S_1} r_2 dS_1 = r_1 r_2 |\Omega|$ , the global roughness is  $r = r_1 r_2$ . The essential property here is that the roughness  $r_2$  of  $dS_1$  is independent of  $dS_1$  and in particular independent of the orientation of  $dS_1$  with respect to the macroscopic surface.

One can construct periodic surfaces with two scales not separated by an order of magnitude, keeping the property that the roughness  $r_2$  of  $dS_1$  is independent of  $dS_1$ , where now  $dS_1$  is not infinitesimal but is a face of a cell. The following construction is inspired by fractals. The elementary cell is a square of side  $a$  (Fig. 1). The first scale of roughness is a pillar of square section of side  $a_1$  and height  $b_1$  placed at the center. This gives a roughness  $r_1 = 1 + 4a_1 b_1 / a^2$ . The surface can now be seen as the union of 13 squares or rectangles: one square of side  $a_1$ , 4 squares of side  $(a - a_1)/2$ , 4 rectangles  $a_1 \times (a - a_1)/2$  and the 4 vertical rectangles  $a_1 \times b_1$ . A second scale of roughness is introduced by placing a pillar of square section of side  $a_2$  and suitable height at the center of each of the 13 faces of the first scale. The height of the pillar will be in proportion of the area of the host face, which may be difficult in the laboratory but may be similar to some cases that occur in Nature. Here the square face of side  $a_1$  will host a pillar of height  $b_2$ ; the vertical rectangles  $a_1 \times b_1$  will host pillars of height  $b_2' = b_2 b_1 / a_1$ ; the rectangles  $a_1 \times (a - a_1)/2$  will host pillars of height  $b_2'' = b_2 (a - a_1) / (2a_1)$ ; and the square faces of side  $(a - a_1)/2$  will host pillars of height  $b_2''' = b_2 (a - a_1)^2 / (4a_1^2)$ . Now all 13 faces have a roughness

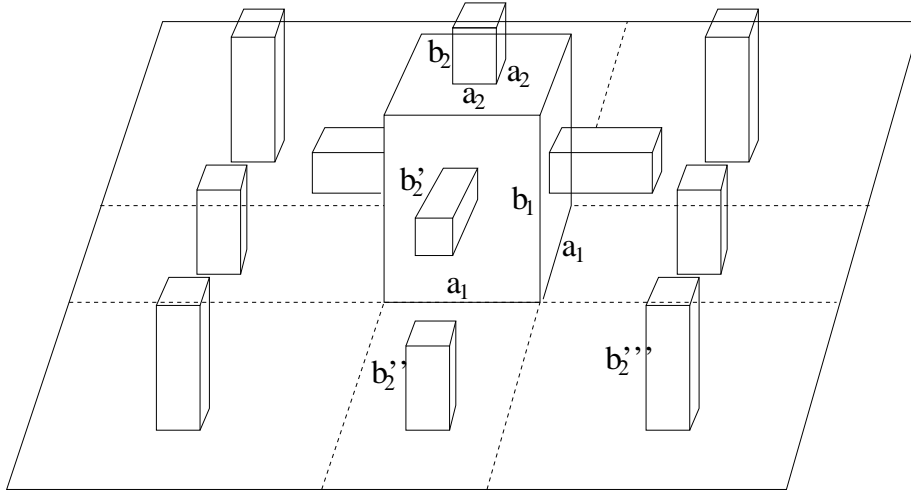


Figure 1: Cell of a periodic substrate with  $r = r_1 r_2$

**r1r2**

$r_2 = 1 + 4a_2 b_2 / a_1^2$ . Therefore the composite elementary cell and the resulting periodic substrate have a roughness  $r = r_1 r_2$ .

A special case is  $a_1 = a/3$ ,  $b_1 = a_1$ ,  $a_2 = a_1/3$ ,  $b_2 = a_2$ , giving  $r_1 = r_2 = 13/9$  (Fig. 2). Iterating indefinitely produces the 3D quadratic Koch surface (type 1) [21], of Hausdorff dimension  $\log(13)/\log(3) \simeq 2.3347$  [22], and infinite Wenzel roughness. After  $n$  iterations the true area is  $(13/9)^n a^2$ . When applied to wetting substrates, the number of iterations is limited by the definition of surface tension:  $(1/3)^n a$  should be larger than a few nm to allow a continuum description of the liquid.

Disorder can be introduced in the quadratic Koch surface by growing the pillars each time with probability  $p$  independently, as after (2), now leading to a Wenzel roughness  $r_1 = 1 + 4p/9$  at the first scale and  $r = r_1 r_2 = (1 + 4p/9)^2$  with two scales. The crucial property to obtain the product of roughnesses is that the random numbers of different scales be independent, because they come up multiplied. On the other hand the random numbers attached to different faces of the same scale are chosen identically distributed but not necessarily independent: indeed they come up together in a sum to which we want to apply the law of large numbers. So at the same scale only asymptotic independence at large distances is required. In the example, faces belonging to the same pillar are dependent, and in fact share a common random number, but faces belonging to different pillars are independent.

In order to obtain hydrophobic substrates, one may prefer  $a_1 < a/3$  and  $b_1 > a_1$ , and then  $a_2, b_2$  taking care to avoid intersection of pillars. A sufficient condition is  $a_1 + 4b_1 b_2 / a_1 + 2a_2 < a$ . An example is  $a_1 = a/5$ ,  $b_1 = 2a_1$ ,  $a_2 = a_1/5$ ,  $b_2 = 2a_2$ , with  $r_1 = r_2 = 33/25$ .

Some disorder can be introduced: suppose the height of each pillar is multi-

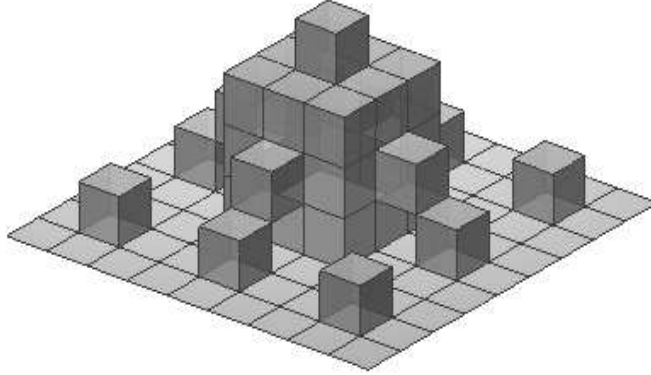


Figure 2: Quadratic Koch surface [21]

koch2

plied by an independent copy of a random variable  $\xi$  of mean 1 and sufficiently narrow support around 1. Let  $S^{(1,2)}$  denote the 2-scale random surface (and its area) over the elementary square  $a \times a$ ; let  $S_i^{(2)}$  for  $i = 1 \dots 13$  denote the random surface over the  $i$ -th square or rectangle  $S_i^{(1)}$  constructed on the first scale. Then

$$S^{(1,2)} = \sum_{i=1}^{13} S_i^{(2)} = \sum_{i=1}^{13} \left( S_i^{(1)} + 4a_2 b_{2,i}(\xi^{(1)}) \xi_i^{(2)} \right) \quad (4)$$

where  $b_{2,i}$  is one of  $b_2$ ,  $b'_2(\xi^{(1)})$ ,  $b''_2$ ,  $b'''_2$  where  $b'_2(\xi^{(1)}) = b_2 b_1 \xi^{(1)} / a_1$ , and  $\xi^{(1)}$  and the  $\xi_i^{(2)}$ 's are independent copies of  $\xi$ . The average over  $\xi^{(2)}$  reads

$$\mathbb{E}^{(2)} S^{(1,2)} = \sum_{i=1}^{13} \left( S_i^{(1)} + 4a_2 b_{2,i}(\xi^{(1)}) \right) = \sum_{i=1}^{13} r_2 S_i^{(1)} \quad (5)$$

where  $r_2 = 1 + 4a_2 b_2 / a_1^2$  and

$$\mathbb{E}^{(1)} \mathbb{E}^{(2)} S^{(1,2)} = r_2 \sum_{i=1}^{13} \mathbb{E}^{(1)} S_i^{(1)} = r_1 r_2 a^2. \quad (6)$$

where  $r_1 = 1 + 4a_1 b_1 / a^2$ . Since  $b_1$  and  $b_2$  are now the average heights, the quantities  $r_1$  and  $r_2$  are the one-scale roughnesses as in (2), and the 2-scale substrate has roughness  $r = r_1 r_2$ .

The law  $r = r_1 r_2$  is linked to scale invariance and isotropy, like fractals, as opposed to urban landscape with terrasses playing a different role than the

walls, which may be self-affine but not fully self-similar. We have put emphasis on block geometries for comparison with the following, but one or two iterations of the triangular Koch surface works as well as a guide to define a 2-scale surface of Wenzel roughness  $r = r_1 r_2$ .

**r1r21**

## 2.2 Two scales of roughness, $r = r_1 + r_2 - 1$ ?

Let us now consider surfaces made of vertical and horizontal pieces only,  $S = S_{\text{horiz}} \cup S_{\text{vert}}$ . We assume also that the surface is given by a height function like in columnar Solid-On-Solid models: overhangs are forbidden. The height function is piecewise constant, and equals zero at the boundary. The jumps define walls, making up  $S_{\text{vert}}$ . The macroscopic reference surface is plane, as before, and by convention horizontal. Then

$$r = \frac{|S|}{|S_{\text{horiz}}|} = 1 + \frac{|S_{\text{vert}}|}{|S_{\text{horiz}}|} \quad (7)$$

The formula can be applied to one-scale roughness, as in (1)(2), with the same result. On the other hand, two-scale roughness will be different: the vertical parts of the first scale cannot be made rough at the smaller scale because this would produce overhangs. Vertical parts can be added, but the total horizontal area always remains equal to the reference area. Therefore

$$\begin{aligned} S^{(1)} &= S_{\text{horiz}}^{(1)} \cup S_{\text{vert}}^{(1)} \\ S^{(1,2)} &= (S_{\text{horiz}}^{(2)} \cup S_{\text{vert}}^{(2)}) \cup S_{\text{vert}}^{(1)} \\ r &= \frac{|S_{\text{horiz}}^{(2)}| + |S_{\text{vert}}^{(2)}| + |S_{\text{vert}}^{(1)}|}{|S_{\text{horiz}}^{(1)}|} = 1 + (r_1 - 1) + (r_2 - 1) \end{aligned} \quad (8) \quad \text{r1r2m1}$$

Where we have used  $|S_{\text{horiz}}^{(2)}| = |S_{\text{horiz}}^{(1)}| = |S_{\text{horiz}}|$ . Formula (8) generalizes easily, for  $n$  scales of roughness, to

$$r = 1 + \sum_{i=1}^n (r_i - 1) \quad (9)$$

Embedding or separating different scales of roughness may be tricky when walls of different scales stand one above the other. This question has been addressed in [25] in the context of an SOS model of wetting seen as a cylinders model: any SOS surface with zero boundary condition can be uniquely defined by families of nested cylinders, positive (building up pillars) or negative (digging). The essential condition given in [25], in addition to nestedness, is that the intersection between the vertical parts of any two cylinders must be empty or reduced to a line or a point, not a surface of positive area: a square pillar of the second scale cannot be placed at ground level against a pillar of the first scale, because it would hide part of the vertical exposed solid area of the first scale. Indeed this would spoil (8).

Example 1: Consider the model on Fig. 1 without the  $b'_2$  overhangs. The unit cell has one  $b_1$ -pillar and 9  $b_2$ - or  $b''_2$ - or  $b'''_2$ -pillars. The argument above

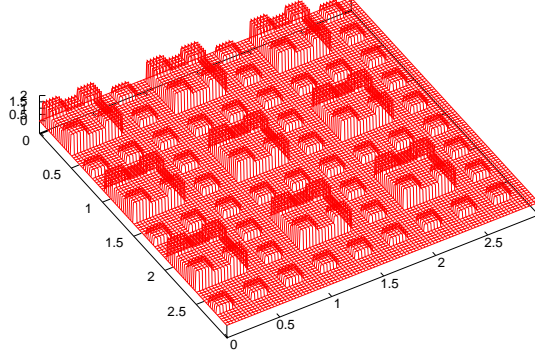


Figure 3:  $r = r_1 + r_2 - 1$

SW

can be applied, with  $r_1$  and  $r_2$  as before, except that the 4 vertical faces of the  $b_1$ -pillar have no roughness. Now we have  $r = r_1 + r_2 - 1 < r_1 r_2$ .

Example 2: Let  $\text{sw}(x) = 2 * \text{floor}(x) - \text{floor}(2 * x) + 1$  denote a square wave of wavelength 1 and amplitude 1, and  $\text{sw}(x, y) = \text{sw}(x) \text{sw}(y)$ . A 2-scale profile

$$z(x, y) = b_1 \text{sw}(x/a_1, y/a_1) + b_2 \text{sw}(x/a_2, y/a_2) \quad (10)$$

sw12

with  $a_2 = a_1/3$  and  $b_2 = b_1/2$  is shown on Fig. 3. Its roughness is

$$r = r_1 + r_2 - 1 = 1 + \frac{2b_1}{a_1} + \frac{2b_2}{a_2} \quad (11)$$

Here  $a_1$  and  $a_2$  are the periods, the respective pillars have side  $a_1/2$  and  $a_2/2$ .

### 3 Cassie-Baxter covered fraction

If the substrate is not completely wet, there is a water-air interface. The pressure difference across the interface is neglected, a good approximation except in cases such as last stages of evaporation, which we don't consider. The interface is then a minimal surface, but not always a plane surface. It may be disconnected into many pieces with different orientations, due to air trapped in anfractuosités.

$$\begin{aligned} F_{SL} &= \gamma_{SL} A_{SL} + \gamma_{SV} (A - A_{SL}) + \gamma_{LV} A_{LV} \\ F_{SV} &= \gamma_{SV} A \\ \cos \theta &= \lim_{\Omega \nearrow \mathbb{R}^2} \frac{F_{SV} - F_{SL}}{|\Omega| \gamma_{LV}} = \cos \theta_0 \lim_{\Omega \nearrow \mathbb{R}^2} \frac{A_{SL}}{|\Omega|} - \lim_{\Omega \nearrow \mathbb{R}^2} \frac{A_{LV}}{|\Omega|} \end{aligned} \quad (12)$$

FSLCBO

If the substrate is sufficiently regular, it may be composed of plane horizontal pieces only, possibly at different heights on the substrate. Or the liquid-vapor



interface may even lie in a unique horizontal plane, whether it be connected or disconnected. Such a configuration is often stable or metastable, with a maximum amount of air trapped, and we then call it a Cassie-Baxter state, in agreement with the simple examples. This section is devoted to Cassie-Baxter states, and to other wetting states with the liquid-vapor interface lying in a unique horizontal plane.

We first define the liquid-vapor interface fraction as the water-air interface area divided by the total projected area,  $\phi_{LV} = |S_{LV}|/|\Omega|$ . The definition is straightforward because  $S_{LV}$  lies in a unique plane.

If the top level of the substrate corresponds to flat roof-tops all at the same height, one may define a Cassie-Baxter state by placing the water-air interface at this top level. The covered (wetted) fraction is then  $\phi = 1 - \phi_{LV}$  and is equal to the top roof-tops area divided by total projected area. The corresponding contact angle  $\theta^{CB}$  is easily shown to obey [24]

$$\cos \theta^{CB} = (1 - \phi) \cos \pi + \phi \cos \theta_0 = -1 + \phi (1 + \cos \theta_0) \quad (13) \quad \boxed{\text{CBflat}}$$

whatever the geometry below the top level roof-tops, assuming some law of large numbers. If the top level of the substrate is rounded, like from coating by spherical nanoparticles, the resulting formula (50) differs from (13). In all cases we define the covered fraction as  $\phi = 1 - \phi_{LV}$ , although it may be smaller than the true wetted area divided by the total projected area. The wetted part or parts of the solid are bounded by triple lines with the air-water interface which is plane. Therefore this wetted part has a well defined Wenzel roughness which we denote  $r^{\text{wet}}$ . Then the wetted area is  $S_{SL} = r^{\text{wet}} \phi |\Omega|$ , and the solid-liquid and solid-vapor free energies are

$$\begin{aligned} F_{SL}^{CB} &= \gamma_{SL} r^{\text{wet}} \phi |\Omega| + \gamma_{LV} (1 - \phi) |\Omega| + \gamma_{SV} (r - r^{\text{wet}} \phi) |\Omega| \\ F_{SV} &= \gamma_{SV} r |\Omega| \end{aligned} \quad (14) \quad \boxed{\text{FSLCB}}$$

leading with Young's equation to a macroscopic contact angle obeying

$$\cos \theta^{CB} = -1 + \phi (1 + r^{\text{wet}} \cos \theta_0) \quad (15) \quad \boxed{\text{thetaCB}}$$

which coincides with formula (2.3) in [23]. Note that the roughness below the level of the air-water interface plays no role. Formula (15) will be applied to pillars of two scales in the next section, and to a substrate coated with spherical nanoparticles in Section 5.1.

### 3.1 Local stability from convexity

**convex**

When there is a liquid-vapour interface at a given height  $z$ , one may ask whether it is a stable or metastable or unstable configuration. The substrate roughness is assumed to be at a scale large compared to the molecular scale, so that a tangent plane to the solid is well defined except at edges and corners, and the angle between the liquid-vapour interface and the solid is well defined except at edges and corners. This angle must everywhere equal the Young angle  $\theta_0$  for

the configuration to be an extremum of the free energy. This local condition depends only upon the substrate geometry around height  $z$  and is therefore unrelated to  $r^{\text{wet}}$  in (15).

Let  $A$  be a point on the solid surface and on the liquid-vapour interface, where they meet at an angle  $\theta_0$ . Consider the vertical plane containing  $A$  and the normal vector to the solid surface at  $A$ . Let  $B$  be a neighboring point in this plane on the solid surface. Consider moving the liquid-vapour interface from  $A$  to  $B$ . Let  $H$  be the projection of  $B$  onto the horizontal plane at  $A$ . The change in free energy, per unit length perpendicular to the given vertical plane, is

$$\pm AH \gamma_{LV} \pm AB (\gamma_{SV} - \gamma_{SL}) \quad (16) \quad \boxed{\text{conv1}}$$

where the signs must be chosen according to whether the corresponding areas increase or decrease. The four cases may be handled one by one, and lead to the same conclusion. Consider the case where  $B$  is higher than  $A$  and the solid surface does not overhang, corresponding to  $\theta_0 \geq \pi/2$ . Then (16) is

$$AH \gamma_{LV} + AB (\gamma_{SV} - \gamma_{SL}) = \gamma_{LV}(AH + AB \cos \theta_0) \quad (17)$$

Now  $AH \simeq AB \cos(\pi - \theta_0)$  and  $AH > AB \cos(\pi - \theta_0)$  if and only if the intersection of the solid with the given vertical plane is strictly convex in a neighborhood of  $A$ . Whence the conclusion:

A liquid-vapour interface at height  $z$  is stable with respect to small fluctuations if and only if (i) it meets the solid at the same angle  $\theta_0$  everywhere along the intersection, and (ii) at any point along the intersection, the intersection of the solid with the vertical plane containing the normal vector is locally strictly convex.

This extends [19] so as to include non-trivial 3D geometries such as shown on Fig.4, or hydrophobic legs of some insects.

Such solids can be constructed as follows. Let  $\rho(z)$ ,  $z \in [0, z_{\max}]$  be a non-negative concave function, with  $\rho(z_{\max}) = 0$ . Let  $\rho_{\max} = \max(\rho)$ . Let  $\mathcal{C}$  be a planar differentiable closed simple curve. For each  $M \in \mathcal{C}$ , let  $M' = M + \rho_{\max} \vec{n}$  be the point at distance  $\rho_{\max}$  from  $M$  on the outer normal to  $\mathcal{C}$  at  $M$ . Let  $\mathcal{C}'$  be the set of such  $M'$ 's. Assume  $d(M', \mathcal{C}) = \rho_{\max}$  for all  $M' \in \mathcal{C}'$ . This is always true when the interior of  $\mathcal{C}$  is a convex set, in particular if the curvature of  $\mathcal{C}$  has a constant sign, positive for definiteness. Otherwise, where the curvature is negative, the radius of curvature should be larger than or equal to  $\rho_{\max}$  in order to satisfy the assumption at least locally.

Embed  $\mathcal{C}$  and  $\mathcal{C}'$  in the plane  $z = 0$  in three-dimensional space. At each point  $M \in \mathcal{C}$ , embed the graph  $\rho(z)$  in the vertical plane containing  $M$  and the normal vector to  $\mathcal{C}$  at  $M$ , with  $\{\rho = 0\}$  as the vertical at  $M$  and  $\rho > 0$  corresponding to the exterior of  $\mathcal{C}$ . Complete the construction of the solid with a roof at height  $z_{\max}$  above the interior of  $\mathcal{C}$ . The projection of the solid onto the horizontal plane coincides with the interior of  $\mathcal{C}'$ .

We call such solids, and limits of such solids, ‘‘vertically convex’’. The roof, which is a translate of the interior of  $\mathcal{C}$ , may be shrunk to a line as in Fig. 4, or to a point, giving a solid with cylindrical symmetry, such as a paraboloid

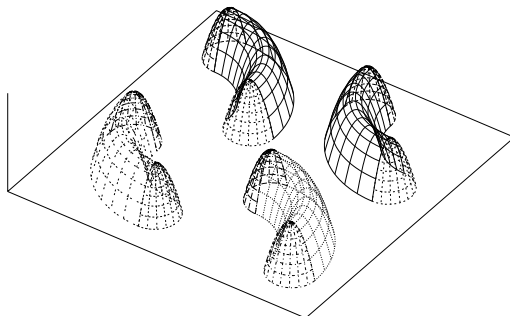


Figure 4: Vertically convex solids

har

of revolution or a sphere. A Cassie-Baxter interface on a periodic or random arrangement of identical vertically convex solids on a plane will be at the unique height  $z(\theta_0)$ , if any, where  $\tan \theta_0 = d\rho/dz$ . Indeed the concavity of  $\rho(z)$  implies that  $d\rho/dz$  is monotone decreasing as a function of  $z$ . The Cassie-Baxter configuration will be locally stable, with (i) and (ii) above satisfied, if  $\rho(z)$  is strictly concave at  $z(\theta_0)$ .

Whether the Cassie-Baxter configuration is stable, being a global minimum of free energy, or metastable, being only a relative minimum, is a global question which can only be decided on a case by case basis. Of course a large  $\theta_0$  favours stability.

Example: consider on a plane a close packing of identical spheres. If  $\theta_0 = \pi/2$ , corresponding to  $\gamma_{SL} = \gamma_{SV}$ , the Cassie-Baxter interface is at the equator of the spheres. The excess in free energy of the Cassie-Baxter configuration relative to the Wenzel configuration comes solely from the small pieces of liquid vapour interface between the spheres,  $(1 - \frac{\pi}{2\sqrt{3}})\gamma_{LV} \simeq 0.093\gamma_{LV}$  per unit area. This is to be compared to the free energy barrier along a homogeneous path from Cassie-Baxter to Wenzel,  $\gamma_{LV}$  per unit area. The Cassie-Baxter configuration is metastable, protected by a significant free energy barrier. The resulting contact angle is  $\cos \theta^{CB} = -1 + \frac{\pi}{2\sqrt{3}}$ , giving  $\theta^{CB} \simeq 95^\circ$ . The Wenzel configuration, with  $\theta^W = 90^\circ$ , is the stable configuration.

The picture changes continuously when  $\theta_0$  is varied in a neighborhood of  $\pi/2$ . When  $\theta_0 > \pi/2$ , the stable "Wenzel" configuration becomes composite, with air trapped at the bottom of the spheres, and the corresponding  $\theta^W$  as (53). When  $\theta_0 < \pi/2$ , the metastable Cassie-Baxter configuration can give a slight hydrophobicity with a slightly hydrophilic material.

### 3.2 Two scales of roughness, $\phi = \phi_1\phi_2$ ?

Here we investigate whether  $\phi = \phi_1\phi_2$  for Cassie-Baxter wetting of 2-scale substrates for which we have obtained the roughness  $r = r_1 + r_2 - 1$ . We restrict further as follows: each of the two scales alone has a unique height,  $b_1$  for scale 1 and  $b_2 < b_1$  for scale 2, so that

$$\begin{aligned} S_{\text{horiz}}^{(1)} &= S_{\text{horiz}}^{(1,z=0)} \cup S_{\text{horiz}}^{(1,z=b_1)}, & \phi_1 &= |S_{\text{horiz}}^{(1,z=b_1)}|/|S_{\text{horiz}}| \\ S_{\text{horiz}}^{(2)} &= S_{\text{horiz}}^{(2,z=0)} \cup S_{\text{horiz}}^{(2,z=b_2)}, & \phi_2 &= |S_{\text{horiz}}^{(2,z=b_2)}|/|S_{\text{horiz}}| \end{aligned} \quad (18)$$

Applying roughness 2 on top of roughness 1 then gives

$$\begin{aligned} S_{\text{horiz}}^{(1,2)} &= S_{\text{horiz}}^{(1,2,z=0)} \cup S_{\text{horiz}}^{(1,2,z=b_1)} \cup S_{\text{horiz}}^{(1,2,z=b_2)} \cup S_{\text{horiz}}^{(1,2,z=b_1+b_2)} \\ S_{\text{horiz}}^{(1,2,z=0)} &= S_{\text{horiz}}^{(1,z=0)} \cap S_{\text{horiz}}^{(2,z=0)}, & S_{\text{horiz}}^{(1,2,z=b_1)} &= S_{\text{horiz}}^{(1,z=b_1)} \cap S_{\text{horiz}}^{(2,z=0)}, \\ S_{\text{horiz}}^{(1,2,z=b_2)} &= S_{\text{horiz}}^{(1,z=0)} \cap S_{\text{horiz}}^{(2,z=b_2)}, & S_{\text{horiz}}^{(1,2,z=b_1+b_2)} &= S_{\text{horiz}}^{(1,z=b_1)} \cap S_{\text{horiz}}^{(2,z=b_2)} \end{aligned} \quad (19)$$

The water-air interface in the true Cassie-Baxter state on the 2-scale substrate will be at height  $b_1 + b_2$ , and the corresponding covered fraction is

$$\phi = \frac{|S_{\text{horiz}}^{(1,2,z=b_1+b_2)}|}{|S_{\text{horiz}}|} = \frac{|S_{\text{horiz}}^{(1,z=b_1)} \cap S_{\text{horiz}}^{(2,z=b_2)}|}{|S_{\text{horiz}}|} \quad (20)$$

The question now is whether the intersection is in proportion. If

$$|S_{\text{horiz}}^{(1,z=b_1)} \cap S_{\text{horiz}}^{(2,z=b_2)}| = \frac{|S_{\text{horiz}}^{(1,z=b_1)}|}{|S_{\text{horiz}}|} |S_{\text{horiz}}^{(2,z=b_2)}| \quad (21)$$

hypfi12

then  $\phi = \phi_1\phi_2$  follows. For example, if the two scales are well separated and the second roughness is applied uniformly over all horizontal parts of the first scale, then (21) and  $\phi = \phi_1\phi_2$  hold true to a good approximation. On the other hand, on a periodic substrate where the elementary cell has only a few pillars, then (21) may be wrong by a large error. This is the case in the example of Fig. 3 corresponding to (10). But the proportion can be respected: instead of (10) with  $a_2 = a_1/3$ , choose

$$z(x, y) = b_1 \text{sw}(x/a_1, y/a_1) + b_2 \text{sw}(x/a_2 - 1/8, y/a_2 - 1/8) \quad (22)$$

sw128

with  $a_2 = a_1/4$ , still giving  $r = r_1 + r_2 - 1$  but now also  $\phi = \phi_1\phi_2$  because the surfacic density of pillars at the second scale is the same on the roof-tops of the first scale as on the pavement.

On such a substrate there is a Wenzel state with the interface at height 0, which we denote  $W_{12}$ ; there is a Cassie-Baxter state at height  $b_1 + b_2$ , which we denote  $CB_{12}$ ; there is also a mixed state at height  $b_1$ , which we denote  $CB_1W_2$  because the second scale of roughness on top of the first is completely wet. Then

the usual formula for the Wenzel state, and (15) applied to the other two states give

$$\begin{aligned}\cos \theta^{W_{12}} &= (r_1 + r_2 - 1) \cos \theta_0 \\ \cos \theta^{CB_{12}} &= -1 + \phi_1 \phi_2 (1 + \cos \theta_0) \\ \cos \theta^{CB_1 W_2} &= -1 + \phi_1 (1 + r_2 \cos \theta_0)\end{aligned}\tag{23} \quad \boxed{\text{CB1W2a}}$$

It is worth noting that the  $CB_1W_2$  configuration for substrate (22) is stable or metastable, because the liquid-vapor interface is plane and is bounded by substrate edges and therefore locally minimal. On the contrary a stable or metastable  $CB_1W_2$  configuration for substrate (10) cannot be planar because the tentative plane meets vertical parts of substrate at an angle  $\pi/2$ , in general different from the required  $\theta_0$ , away from edges (see Fig. 3).

## 4 Separation of scales

### 4.1 Two-scale affine roughness

Consider a two-scale substrate obeying the hypotheses of Subsections (2.2) and (3.2), so that

$$\begin{aligned}\cos \theta^{W_{12}} &= r \cos \theta_0, \quad r = r_1 + r_2 - 1 \\ \cos \theta^{CB_{12}} &= -1 + \phi (1 + \cos \theta_0), \quad \phi = \phi_1 \phi_2\end{aligned}\tag{24} \quad \boxed{\text{CB12W12}}$$

Instead of using the composite  $r$  and  $\phi$ , one can write (24) as a composition rule for contact angles:

$$\begin{aligned}\cos \theta^{W_1 X_2} &= (r_1 - 1) \cos \theta_0 + \cos \theta^{X_2} \tag{25} \quad \boxed{\text{W1X2}} \\ \cos \theta^{CB_1 X_2} &= -(1 - \phi_1) + \phi_1 \cos \theta^{X_2} \tag{26} \quad \boxed{\text{CB1X2}}\end{aligned}$$

(25)(26) follows from (24) with corresponding choices  $X = W$  or  $X = CB$ , but can also be derived directly and applied to any wetting state at scale 2 whenever the corresponding contact angle is known. Indeed  $\cos \theta$  is minus the specific excess solid-liquid free energy relative to the solid-vapor free energy, in units of  $\gamma_{LV}$ . And of course  $\cos \theta_0$  is the same for the smooth solid. Then the first term in (25) is easily identified with the vertical contribution, and the second term with the horizontal contribution; the first term in (25) is the liquid-vapor contribution, and the second term is the horizontal wetted top contribution.

Consider also the  $CB_1W_2$  and  $W_1CB_2$  configurations which are ‘‘Cassie-Baxter’’ at scale 1 and ‘‘Wenzel’’ at scale 2 or conversely. Separation of scales occurs when the thermodynamic limit is achieved for scale 2 roughness on each motif of scale 1 roughness. In particular scale 2 motives at the boundaries of scale 1 motives are negligible with respect to the bulk. In this limit the curved parts of  $CB_1W_2$  and  $W_1CB_2$  liquid-vapor interfaces are negligible. Indeed these curved parts border scale 2 motives at the boundaries of scale 1 motives. Therefore (15)(23) apply,

$$\cos \theta^{CB_1 W_2} = -1 + \phi_1 (1 + r_2 \cos \theta_0)\tag{27} \quad \boxed{\text{CB1W2b}}$$

And, using (14) at scale 2, in terms of free energy densities  $f = \lim_{\Omega \nearrow \mathbb{R}^2} F/|\Omega|$ ,

$$\begin{aligned} f_{SL}^{W_1CB_2} &= \phi_2 \gamma_{SL} + (r_2 - \phi_2) \gamma_{SV} + (1 - \phi_2) \gamma_{LV} + (r_1 - 1) \gamma_{SL} \\ f_{SV} &= (r_1 + r_2 - 1) \gamma_{SV} \end{aligned} \quad (28)$$

leading to

$$\cos \theta^{W_1CB_2} = (r_1 - 1 + \phi_2) \cos \theta_0 - 1 + \phi_2 \quad (29)$$

W1CB2

Example [27]:  $\theta_0 = 108^\circ$ , scale 1 is a square array of discs of diameter  $15 \mu\text{m}$  and height  $2 \mu\text{m}$ , with pitch  $30 \mu\text{m}$ , leading to  $r_1 = 1.1$ . Scale 2 is a square array of discs of diameter  $230 \text{ nm}$  and height  $500 \text{ nm}$ , with pitch  $430 \text{ nm}$ , leading to  $r_2 = 2.95$ , and  $\phi_2 = 0.22$  in the  $CB_2$  configuration. The combined roughness is  $r_1 + r_2 - 1 = 3.05$ , and (29) gives  $\theta^{W_1CB_2} = 151^\circ$ , winning over the other wetting states, from (24)(27):  $\theta^{W_{12}} = 161^\circ$ ,  $\theta^{CB_{12}} = 166^\circ$ ,  $\theta^{CB_1W_2} = 169^\circ$ .

The authors of [27] find the same angle doing a computation in finite volume, and without assuming separation of scales. They do not however include macroscopic boundary corrections associated with line tension nor scale 1 boundary corrections due partly to the fact that the larger pitch is not a multiple of the smaller, and partly due to the fact that the liquid vapor interface must be curved on the boundary of scale 1 discs. They remark that the value  $151^\circ$  is less than the value  $160^\circ$  found experimentally [5] for a substrate of similar roughness. The substrate in the experiment, however, looks multi-scale rather than 2-scale.

## 4.2 Three-scale affine roughness

The method easily extends to three well separated scales of roughness. At each scale wetting can be 'Cassie-Baxter' or 'Wenzel', hence  $2^3 = 8$  states of wetting, with the following Young angles, the smallest of which is associated with the stable configuration:

$$1 + \cos \theta^{CB_{123}} = \phi_3(1 + \cos \theta^{CB_{12}}) \quad (30)$$

$$1 + \cos \theta^{CB_{12}W_3} = \phi_1 \phi_2(1 + \cos \theta^{W_3}) \quad (31)$$

$$1 + \cos \theta^{CB_1W_2CB_3} = \phi_1(1 + \cos \theta^{W_2CB_3}) \quad (32)$$

$$1 + \cos \theta^{W_1CB_{23}} = \phi_2 \phi_3(1 + \cos \theta_0) + (r_1 - 1) \cos \theta_0 \quad (33)$$

$$1 + \cos \theta^{CB_1W_{23}} = \phi_1(1 + \cos \theta^{W_{23}}) \quad (34)$$

$$1 + \cos \theta^{W_{12}CB_3} = \phi_3(1 + \cos \theta_0) + (r_1 + r_2 - 2) \cos \theta_0 \quad (35)$$

$$1 + \cos \theta^{W_1CB_2W_3} = \phi_2(1 + \cos \theta_0) + (r_1 - 1 + \phi_2(r_3 - 1)) \cos \theta_0 \quad (36)$$

$$1 + \cos \theta^{W_{123}} = 1 + (r_1 + r_2 + r_3 - 2) \cos \theta_0 \quad (37)$$

Fig. 5 shows  $\cos \theta$  function of  $\cos \theta_0$  for the eight wetting states, together with a one-scale substrate of same Wenzel roughness. The aspect ratios height/radius of cylinders making up the substrate on each scale are the same. The roughness is  $r_1 = r_2 = r_3 = 1.75$ , the covered fractions  $\phi_1 = \phi_2 = \phi_3 = 0.25$ .

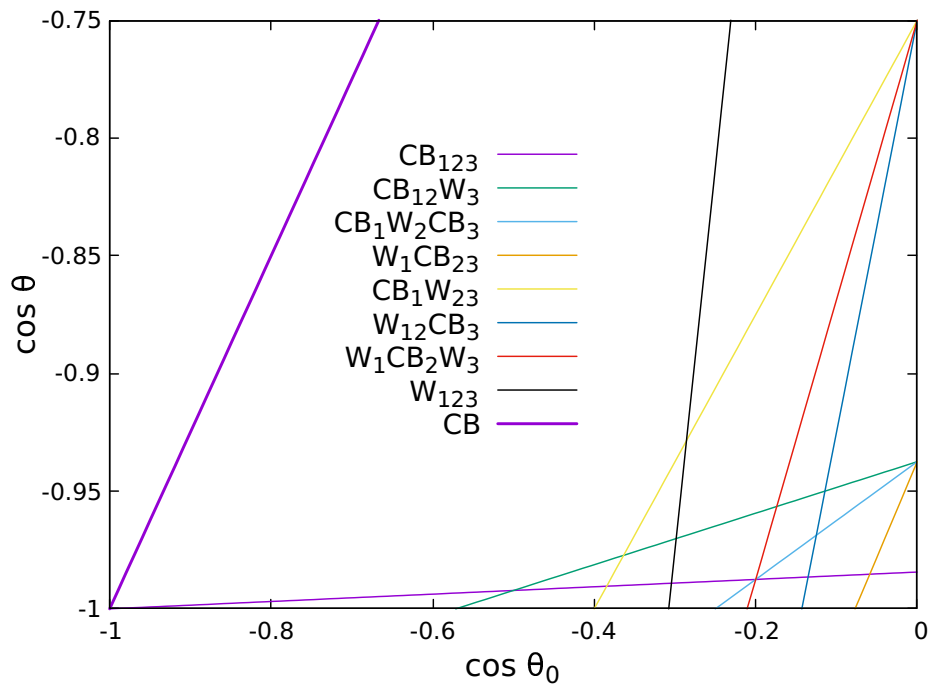


Figure 5: Eight wetting states with  $r = r_1 + r_2 + r_3 - 2$ , and 1-scale  $CB$

123

### 4.3 Isotropic roughness

Consider a two-scale substrate obeying the main hypothesis of Subsection (2.1): any surface element  $dS_1$ , infinitesimal at the larger scale, has a true area  $r_2 dS_1$  when the smaller scale '2' is taken into account. Suppose that the Young angle  $\theta^{X_2}$  in a wetting state  $X$  for scale 2 roughness alone is known, so that the corresponding free energy density is

$$f_{SL}^{X_2} = r_2 \gamma_{SV} - \cos \theta^{X_2} \gamma_{LV} \quad (38)$$

Then

$$\cos \theta^{W_1 X_2} = \frac{r_1 r_2 \gamma_{SV} - r_1 f_{SL}^{X_2}}{\gamma_{LV}} = r_1 \cos \theta^{X_2} \quad (39) \quad \boxed{W1X2I}$$

giving

$$\cos \theta^{W_{12}} = r_1 \cos \theta^{W_2} = r_1 r_2 \cos \theta_0 \quad (40)$$

Suppose in addition that  $\theta^{CB_2}$  obeys (13). Then

$$\cos \theta^{W_1 CB_2} = r_1 \cos \theta^{CB_2} = -r_1 + r_1 \phi_2 + r_1 \phi_2 \cos \theta_0 \quad (41)$$

Consider now the  $CB_{12}$  and  $CB_1 W_2$  configurations, denoted  $CB_1 X_2$  with  $X = CB$  or  $X = W$ :

$$f_{SL}^{CB_1 X_2} = r_1^{\text{wet}} \phi_1 f_{SL}^{X_2} + (r - r^{\text{wet}} \phi_1) \gamma_{SV} + (1 - \phi_1) \gamma_{LV} \quad (42)$$

leading to

$$\cos \theta^{CB_1 X_2} = -1 + \phi_1 (1 + r_1^{\text{wet}} \cos \theta^{X_2}) \quad (43) \quad \boxed{CB1X2I}$$

Formulas (39)(43) agree with formulas previously derived for simple geometries [26], and may be applied in more complex situations.

*Paraboloids:*

Consider at scale 1 a roughness made of paraboloids of revolution  $z = z_0 - (x^2 + y^2)/2a$ , centered on an array or a random set of points with density  $\rho$ , all rounded tops at the same  $z_0$  with the same radius of curvature  $a$  at the top. In state  $CB_1$ , with the liquid-vapor interface meeting the paraboloids at an angle  $\theta^{X_2}$ , the covered fraction and wet roughness are

$$\phi_1 = \pi a^2 (\tan \theta^{X_2})^2 \rho, \quad r_1^{\text{wet}} = -\frac{2}{3} \frac{1 + (\cos \theta^{X_2})^3}{\cos \theta^{X_2} (\sin \theta^{X_2})^2} \quad (44)$$

where we used the area of the paraboloid cap as

$$\frac{\pi}{6a^2} \left( -\frac{1}{(\cos \theta^{X_2})^3} - 1 \right) \quad (45)$$

*Raspberries:*

A close packing of raspberry-like particles, with the smaller particles also close-packed, in the separation of scales limit, obeys (51) iterated once:

$$\cos \theta^{CB_{12}} = -1 + \frac{\pi^3}{24\sqrt{3}} (1 + \cos \theta_0)^4 \quad (46) \quad \boxed{CB12close}$$



giving  $\theta^{CB_{12}} = 144^\circ$  when  $\theta_0 = 107^\circ$ . If the smaller particles are not close-packed then  $CB_1W_2$  may win. For a density of the smaller particles equal to 0.5 divided by the area of an equilateral triangle of side  $3R_2$ , giving  $\theta^{W_2} = 138^\circ$  (see after (53)), (51) with 138 instead of 107 gives  $\theta^{CB_1W_2} = 160^\circ$ .

## 5 Cylindrical symmetry

Minimal surfaces with cylindrical symmetry are defined by ordinary differential equations, much easier mathematically than the more general partial differential equations.

spheres

### 5.1 Monodisperse spherical nanoparticles

Let us recall and reformulate in more generality some results for spherical nanoparticles [18]. The Wenzel state is not completely Wenzel when  $\theta_0 > \pi/2$  because some air is always trapped near the basis of the spheres. We don't have a general formula to take it into account, but the cylindrical symmetry allows an explicit computation of the corresponding almost-Wenzel contact angle. And the top level is rounded, so that the Cassie-Baxter contact angle must be computed with (15) instead of the usual simpler formula (13).

The random arrangement of nanoparticles makes a random triangulation of the plane, with the centers of the spheres as vertices of the triangulation. Consider an area  $A$  with  $N$  nanoparticles,  $A, N \rightarrow \infty$  with  $4\pi R^2 N/A \rightarrow r - 1$ . We assume that the disorder allows to apply the law of large numbers, giving such a convergence and giving also the number of triangles as approximately twice the number of particles. Then, with  $\sim$  from the law of large numbers,

$$\begin{aligned}
F_{SV}^{rr}(A) &\sim (A + 4\pi R^2 N)\gamma_{SV} \\
F_{SL}^{CB}(A) &\sim (A + 2\pi(1 - \cos \theta_0)R^2 N)\gamma_{SV} + \\
&\quad + 2\pi(1 + \cos \theta_0)R^2 N\gamma_{SL} + (A - \pi R^2 \sin^2 \theta_0 N)\gamma_{LV} \\
F_{SL}^W(A) &\sim \left(\pi\rho_0^2 + 2\pi(R^2 - R\sqrt{R^2 - \rho_1^2})\right)N\gamma_{SV} + \\
&\quad + \left(A - \pi\rho_0^2 + 2\pi(R^2 + R\sqrt{R^2 - \rho_1^2})\right)\gamma_{SL} + A_{\text{cat}}N\gamma_{LV} \tag{47}
\end{aligned}$$

where  $\rho_1$  and  $\rho_0$  are the catenoid radii on the sphere and the plane respectively, and  $A_{\text{cat}}$  is the catenoid area between heights 0 and  $z_1$ ,

$$A_{\text{cat}} = \pi\rho_c^2 \left( \frac{z_1}{\rho_c} + \frac{1}{2} \sinh \frac{2z_c}{\rho_c} + \frac{1}{2} \sinh \frac{2z_1 - 2z_c}{\rho_c} \right) \tag{48}$$

In the Cassie-Baxter state, the covered fraction  $\phi = 1 - \phi_{LV}$  and wetted roughness  $r^{\text{wet}}$  are

$$\phi = \frac{1}{4}(r - 1) \sin^2 \theta_0$$

$$r^{\text{wet}} = \frac{2(1 + \cos \theta_0)}{\sin^2 \theta_0} \quad (49)$$

so that applying (15) gives

$$\cos \theta^{CB} = -1 + \frac{1}{4}(r-1)(1 + \cos \theta_0)^2 \quad (50) \quad \boxed{\text{CBsph}}$$

For close packing,  $r = 1 + 2\pi/\sqrt{3}$ ,

$$\cos \theta^{CB} = -1 + \frac{\pi}{2\sqrt{3}}(1 + \cos \theta_0)^2 \quad (51) \quad \boxed{\text{CBclose}}$$

giving  $\theta^{CB} = 123^\circ$  when  $\theta_0 = 107^\circ$ . Given  $\theta_0$ , close packing minimizes  $\theta^{CB}$  and maximizes the stability of the  $CB$  configuration.

The almost-Wenzel configuration is more complicated:

$$\begin{aligned} A^{-1}F_{SV}^{rr}(A) &\sim r \gamma_{SV} \\ A^{-1}F_{SL}^W(A) &\sim \frac{1}{4}(\hat{\rho}_0^2 + 2(1 - \sqrt{1 - \hat{\rho}_1^2}))(r-1)\gamma_{SV} + \gamma_{SL} \\ &\quad - \frac{1}{4}(\hat{\rho}_0^2 - 2(1 - \sqrt{1 - \hat{\rho}_1^2}))(r-1)\gamma_{SL} + \frac{\hat{A}_{\text{cat}}}{4\pi}(r-1)\gamma_{LV} \end{aligned} \quad (52) \quad \boxed{\text{F3D1}}$$

where  $\hat{\rho}_1$  and  $\hat{\rho}_0$  and  $\hat{A}_{\text{cat}}$  should now be computed for a sphere of radius one and are functions of  $\theta_0$  only. Then

$$\begin{aligned} \cos \theta^W &= r \cos \theta_0 + \frac{1}{4}(\hat{\rho}_0^2 + 2(1 - \sqrt{1 - \hat{\rho}_1^2})) \cos \theta_0 (r-1) - \frac{\hat{A}_{\text{cat}}}{4\pi}(r-1) \\ &> r \cos \theta_0 \end{aligned} \quad (53) \quad \boxed{\text{Wsph}}$$

For a density of nanoparticles equal to 0.5 divided by the area of an equilateral triangle of side  $3R$ , giving  $r = 1 + \frac{8\pi}{9\sqrt{3}}$ , and  $\theta_0 = 107^\circ$ , (53) gives  $\theta^W = 138^\circ$ , winning over  $\theta^{CB} = 142^\circ$ .

The Wenzel contact angle  $\theta^W$  is a little smaller but very near the approximation  $r \cos \theta_0$ , at least when  $\theta_0$  is not much bigger than  $\pi/2$ . If either the Cassie-Baxter configuration or the Wenzel configuration minimize the energy in every triangle of the triangulation by the nanoparticle centers, then the maximum between  $\cos \theta^{CB}$  and  $\cos \theta^W$  will be the true contact angle. This may be a good approximation away from the value of  $\cos \theta_0$  corresponding to the transition between the two. However, except for periodic substrates, this transition will be smeared by the randomness.

## 5.2 Monodisperse cylindrical pillars

In the case of spherical nanoparticles, whatever  $\pi/2 < \theta_0 < \pi$ , the liquid wets a nontrivial fraction of the sphere, fraction tending to zero when  $\theta_0 \nearrow \pi$  and tending to one when  $\theta_0 \searrow \pi/2$ . On the contrary, in the case of a pillar of finite height, depending upon  $\theta_0$ , the liquid may wet completely the pillar, or

also de-wet completely the vertical surface of the pillar. The transitions can be computed exactly for pillars with cylindrical symmetry.

Indeed the liquid-vapor interface is then again a catenoid as for spherical nanoparticles,  $\rho = \rho_c \cosh((z - z_c)/\rho_c)$ , where the catenoid parameters  $\rho_c, z_c$  have to be computed from the boundary conditions. Gravity is neglected, as before. Consider the case where the triple line is at a height  $z_1$  less than the height of the cylinder. Let  $\rho_0$  be the catenoid radius at the plane substrate,  $z = 0$ . Then we have to solve

$$\begin{aligned} \rho_0 &= \rho_c \cosh \frac{z_c}{\rho_c}, & R &= \rho_c \cosh \frac{z_1 - z_c}{\rho_c} \\ \cot \theta_0 &= -\sinh \frac{z_c}{\rho_c}, & \tan \theta_0 &= \sinh \frac{z_1 - z_c}{\rho_c} \end{aligned} \quad (54) \quad \boxed{\text{cylcat}}$$

which give, using  $(\cosh x)^2 - (\sinh x)^2 = 1$ ,

$$\begin{aligned} \rho_c &= -R \cos \theta_0, & \rho_0 &= -R \cot \theta_0 \\ \frac{z_c}{\rho_c} &= -\sinh^{-1}(\cot \theta_0), & \frac{z_c - z_1}{\rho_c} &= \cosh^{-1}\left(\frac{-1}{\cos \theta_0}\right) > 0 \end{aligned} \quad (55) \quad \boxed{\text{cylsol}}$$

which requires  $\theta_0 > 3\pi/4$  as expected from the minimality of the surface and the boundary conditions.  $\rho_0$  and  $z_1$  vary respectively from  $R$  to  $+\infty$  and from  $0$  to  $+\infty$  as  $\theta_0$  varies from  $3\pi/4$  to  $\pi$ . When  $z_1$  reaches the top of the pillar  $z_1 = b$ , at some  $\theta_0 = \theta_0^b$ , the vertical surface of the pillar is completely de-wetted. When  $\theta_0 > \theta_0^b$ , the top level of the catenoid  $z_1$  remains at  $z_1 = b$ , but the contact angle at the top of the pillar becomes strictly less than  $\theta_0$ , the last equation in (54) is lost. When  $\pi/2 < \theta_0 < 3\pi/4$ , the liquid wets completely the pillar. In summary, starting from  $\theta_0 = \pi/2$ , the liquid wets completely the pillar until  $\theta_0 = 3\pi/4$ , then from  $\theta_0 = 3\pi/4$  to  $\theta_0 = \theta_0^b$  the pillar gradually dewets, and then remains with a completely dewetted vertical surface up to  $\theta_0 = \pi$ .

For  $\pi/2 \leq \theta_0 \leq 3\pi/4$  the Wenzel state is completely Wenzel, so that  $\cos \theta^W = r \cos \theta_0$ . Let us now consider  $3\pi/4 \leq \theta_0 \leq \theta_0^b$  and proceed, as for the spherical nanoparticles, from a triangle in the triangulation by the cylinder centers on the plane substrate.

$$\begin{aligned} F_{SV}^{rr} &= (A_{\text{tri}} + \pi Rb)\gamma_{SV} \\ F_{SL}^W &= \left(\frac{1}{2}\pi(\rho_0^2 - R^2) + \pi R z_1\right)\gamma_{SV} \\ &\quad + \left(A_{\text{tri}} - \frac{1}{2}\pi(\rho_0^2 - R^2) + \pi R(b - z_1)\right)\gamma_{SL} + \frac{1}{2}A_{\text{cat}}\gamma_{LV} \end{aligned} \quad (56) \quad \boxed{\text{FWcyl}}$$

Factors of 1/2 arise because the three angles in the triangle, cutting cylinder and catenoid sectors, sum up to  $\pi$  only. The full catenoid area between heights 0 and  $z_1$  is (48) with (55),

$$A_{\text{cat}} = \pi R^2 \cos^2 \theta_0 \left[ -\cosh^{-1}\left(\frac{-1}{\cos \theta_0}\right) - \sinh^{-1}(\cot \theta_0) - \frac{\cos \theta_0}{\sin^2 \theta_0} - \frac{\sin \theta_0}{\cos^2 \theta_0} \right] \quad (57)$$

which is positive for  $\theta_0 > 3\pi/4$ . From (56) we get for this partially Wenzel state

$$\begin{aligned} \cos \theta^W &= r \cos \theta_0 - \frac{r-1}{2\pi Rb} \left[ 2\pi R z_1 \cos \theta_0 + \pi(\rho_0^2 - R^2) \cos \theta_0 + A_{\text{cat}} \right] \\ &> r \cos \theta_0 \end{aligned} \quad (58)$$

where  $r = 1 + 2\pi RbN/A$ . For comparison, given the flat roof-tops,

$$\cos \theta^{CB} = -1 + \phi^{CB} (1 + \cos \theta_0) \quad (59)$$

with  $\phi^{CB} = \pi R^2 N/A$ .

Let us now consider  $\theta_0^b < \theta_0 < 3\pi/4$ . The second and third equations in (54) with  $z_1 = b$  give an equation for  $\rho_c$  alone,

$$R = \rho_c \left( \cosh \frac{b}{\rho_c} \right) \frac{1}{\sin \theta_0} + \rho_c \left( \sinh \frac{b}{\rho_c} \right) \cot \theta_0 \quad (60)$$

and then  $\rho_0 = \rho_c / \sin \theta_0$  and  $z_c = \rho_c \cosh^{-1}(1/\sin \theta_0)$  and from (56) with  $z_1 = b$ ,

$$\cos \theta^W = \cos \theta_0 - \pi(\rho_0^2 - R^2) \cos \theta_0 \frac{N}{A} - A_{\text{cat}} \frac{N}{A} \quad (61)$$

where  $N/A = (r-1)/(2\pi Rb)$  and  $A_{\text{cat}}$  is (48) with  $z_1 = b$ .

**Acknowledgements** The authors thank the European Space Agency (ESA) and the Belgian Federal Science Policy (BELSPO) for their support in the framework of the PRODEX Programme. This research was also partially funded by the FNRS and the Region Wallonne.

## References

- [1] Z. G. Guo, J. Fang, J. C. Hao, Y. M. Liang, W. M. Liu, A Novel Approach to Stable Superhydrophobic Surfaces, *Chem. Phys. Chem.* 7 (2006) 1674-1677.
- [2] J. T. Han, X. R. Xu, K. W. Cho, Diverse Access to Artificial Superhydrophobic Surfaces Using Block Co-polymers, *Langmuir* 21 (2005) 6662-6665.
- [3] H. S. Hwang, S. B. Lee, I. Park, Fabrication of Raspberry-Like Superhydrophobic Hollow Silica Particles, *Mater. Lett.* 64 (2010) 2159-2162.
- [4] Y. H. Huang, J. T. Wu, S. Y. Yang, Direct Fabricating Patterns Using Stamping Transfer Process with PDMS Mold of Hydrophobic Nanostructures on Surface of Micro-Cavity, *Microelectron. Eng.* 88 (2011) 849-854.
- [5] N. J. Shirtcliffe, G. McHale, M. I. Newton, G. Chabrol and C. C. Perry: *Dual-scale roughness produces unusually water repellent surfaces*. *Advanced Materials* 16, 1929-1932, (2004).

- [6] K. K. Lau, J. Bico, K. B. K. Teo, M. Chhowalla, G. A. J. Amaratung, W. I. Milne, G. H. McKinley, K. K. Gleason, Superhydrophobic Carbon Nanotube Forests, *Nano Lett.* **3** (2003) 1701-1705.
- [7] Y.C. Hong, H.S. Uhm, Superhydrophobicity of a material made from multiwalled carbon nanotubes, *Appl. Phys. Lett.* **88** (2006) 244101-244103.
- [8] Z.J. Chen, Y.B. Guo, S.M. Fang, A facial approach to fabricate superhydrophobic aluminum surface, *Surf. Interface Anal.* **42** (2010) 1-6.
- [9] D.K. Sarkar, N. Saleema, One-step fabrication process of superhydrophobic green coatings, *Surf. Coat. Technol.* **204** (2010) 2483-2486.
- [10] A. Nakajima, A. Fujishima, K. Hashimoto, T. Watanabe, Preparation of transparent superhydrophobic boehmite and silica films by sublimation of aluminum acetylacetonate, *Adv. Mater.* **11** (1999) 1365-1368.
- [11] M. Morra, E. Occhiello, F. Garbassi, Contact angle hysteresis in oxygen plasma treated poly (tetrafluoroethylene), *Langmuir* **5** (1989) 872-876.
- [12] J. P. Youngblood, T. J. McCarthy, Ultrahydrophobic polymer surfaces prepared by simultaneous ablation of polypropylene and sputtering of Poly (tetrafluoroethylene) using radio frequency plasma, *Macromolecules* **32** (1999) 6800-6806.
- [13] S. Shibuichi, T. Onda, N. Satoh, T. Kaoru, Super water-repellent surfaces resulting from fractal surfaces. *J. Phys. Chem.* **100** (1996) 19512-19517.
- [14] G. McHale, N. J. Shirtcliffe and M. I. Newton: Super-hydrophobic and super-wetting surfaces: Analytical potential? *Analyst*, 2004, **129**, 284-287
- [15] H-J. Butt, K. Graf, M. Kappl (2005) *Physics and chemistry of interfaces.* Wiley-VCH, Weinheim
- [16] Hui-Jung Tsai and Yuh-Lang Lee: Facile Method to Fabricate Raspberry-like Particulate Films for Superhydrophobic Surfaces. *Langmuir* 2007, **23**, 25, 12687–12692
- [17] J. De Coninck, F. Dunlop, Th. Huillet: *Wetting in 1+1 dimensions with two-scale roughness.* *Physica A.*, **438**, 398-415 (2015).
- [18] J. De Coninck, F. Dunlop, Th. Huillet: *Is superhydrophobicity robust with respect to disorder?* *Eur. Phys. J. E* **36**, 104 (2013).
- [19] A. Marmur: *Wetting on hydrophobic rough surfaces: to be heterogeneous or not to be?* *Langmuir* **19**, 8343–8348 (2003).
- [20] W. Ming, D. Wu, R. van Benthem, G. de With: *Super- hydrophobic films from raspberry-like particles.* *Nano Lett.* **5**, 2298–2301 (2005).
- [21] [http://en.wikipedia.org/wiki/File:Quadratic\\_Koch\\_3D\\_\(type1\\_stage2\).png](http://en.wikipedia.org/wiki/File:Quadratic_Koch_3D_(type1_stage2).png).

- [22] [http://en.wikipedia.org/wiki/List\\_of\\_fractals\\_by\\_Hausdorff\\_dimension](http://en.wikipedia.org/wiki/List_of_fractals_by_Hausdorff_dimension).
- [23] B. Bhushan, Y.C. Jung, K. Koch: *Micro-, nano- and hierarchical structures for superhydrophobicity, self-cleaning and low adhesion*. Phil. Trans. R. Soc. A **367**, 1631–1672 (2009).
- [24] A. B. D. Cassie, S. Baxter: *Wettability of porous surfaces*. Trans. Faraday Soc **40**, 546–551, (1944).
- [25] E.I. Dinaburg, A.E. Mazel: *Layering transition in SOS model with external magnetic field*. J. Stat. Phys. **74**, 533–563 (1996).
- [26] N. A. Patankar. *Mimicking the lotus effect: influence of double roughness structures and slender pillars*. Langmuir **20**, 8209-8213, (2004).
- [27] S. H. Sajadina, F. Sharif: *Thermodynamic analysis of the wetting behavior of dual scale patterned hydrophobic surfaces*. J. Colloid Interface Sci. **344**, 575–583, (2010).
- [28] R. W. Wenzel: *Resistance of solid surfaces to wetting by water*. Ind. Eng. Chem. **28**, 988–994, (1936).